

# Doping effects on the stacking fault energies of the $\gamma'$ phase in Ni-based superalloys\*

Weijie Li(李伟节)<sup>1,2</sup> and Chongyu Wang(王崇愚)<sup>1,†</sup>

<sup>1</sup>Department of Physics, Tsinghua University, Beijing 100084, China

<sup>2</sup>Institute of Applied Physics and Computational Mathematics, Beijing 100088, China

(Received 7 June 2019; revised manuscript received 13 December 2019; accepted manuscript online 16 December 2019)

The doping effects on the stacking fault energies (SFEs), including the superlattice intrinsic stacking fault and superlattice extrinsic stacking fault, were studied by first principles calculation of the  $\gamma'$  phase in the Ni-based superalloys. The formation energy results show that the main alloying elements in Ni-based superalloys, such as Re, Cr, Mo, Ta, and W, prefer to occupy the Al-site in Ni<sub>3</sub>Al, Co shows a weak tendency to occupy the Ni-site, and Ru shows a weak tendency to occupy the Al-site. The SFE results show that Co and Ru could decrease the SFEs when added to fault planes, while other main elements increase SFEs. The double-packed superlattice intrinsic stacking fault energies are lower than superlattice extrinsic stacking fault energies when elements (except Co) occupy an Al-site. Furthermore, the SFEs show a symmetrical distribution with the location of the elements in the ternary model. A detailed electronic structure analysis of the Ru effects shows that SFEs correlated with not only the symmetry reduction of the charge accumulation but also the changes in structural energy.

**Keywords:** stacking fault energy, site preference, Ni-based superalloys, electronic structure

**PACS:** 64.60.De, 61.72.Nn, 61.72.S-, 61.82.Bg

**DOI:** 10.1088/1674-1056/ab6203

## 1. Introduction

Ni-based superalloys offer an excellent mechanical performance at high temperature, and are widely used in the manufacture of aero engines and turbine blades.<sup>[1]</sup> Ni-based superalloys have a complex constitution, containing more than ten elements, such as, Al, Co, Cr, Mo, Ta, W, Re, Ru, *etc.* Re and Ru are key elements for fourth (5–6 wt% Re, 2–3 wt% Ru) and fifth (5–6 wt% Re, 5–6 wt% Ru) generation superalloys, and Ir addition<sup>[2]</sup> is considered vital to development of sixth generation superalloys. Understanding how elements affect the alloy and their synergistic effect on the material properties remains an important area of Ni-based superalloy research.

Generally, stacking fault energy (SFE) is important in determining the plastic deformation mechanisms in a metal. Dislocations are constrained to move in a more planar fashion in materials with low SFE. In other words, the low SFE restricts dislocation movement and enhances the hardness of the alloys. Others have studied the generalized stacking fault energies of Ni<sub>3</sub>Al<sup>[3]</sup> in the past few years which is also helpful to understand the shearing of the  $\gamma'$  phase. In Ref. [4], the authors investigated the segregation of the main alloying elements in Ni<sub>3</sub>Al. The alloying effect on the SFEs is closely related to its concentrations, site preference, and even with the models used in the calculations. Yu<sup>[3]</sup> calculated elemental effects on the generalized planar fault curves in Ni<sub>3</sub>Al by slip modelling. With modern computational power, the number of layers should be large enough to allow us to ignore interactions

with the stacking faults, or the interactions between vacuum layer and stacking fault. This work is focused on the alloying elements effects, including the types and sites of the alloying element, on SFEs in the  $\gamma'$  phases of Ni-based superalloys. In addition, we analyzed the energies, electronic structure, and physical basis for the results, thus furnishing information valuable to alloy design.

## 2. Method and calculation

As [111] is the close-packed direction in an fcc crystal, the models were constructed with [1 $\bar{1}$ 0], [11 $\bar{2}$ ], and [111] directions. A 15-Å wide vacuum layer was added to each model to separate the stacking faults (SF), as shown in Fig. 1. In Fig. 1(a), the superlattice intrinsic stacking fault (SISF) model has 112 atoms. The superlattice intrinsic stacking fault with ABAB repeat layers (SISF2) and superlattice extrinsic stacking fault (SESF) with 128 atoms are shown in Figs. 1(b) and 1(c). The alloying elements were adopted in the No. 3, No. 5, and No. 5 layers in Figs. 1(a)–1(c), respectively. Furthermore, the elements were also adopted in 0 to 9 layers when calculating the effects of the distance between alloying element and SF on the SFEs. During the calculation, the three layers near the vacuum were totally fixed during relaxation to avoid surface reconfiguration, while atoms on other layers were totally relaxed, including the layer distance and atom position.

To obtain total energies, density functional theory (DFT) calculations are implemented using the Vienna *Ab initio* Sim-

\*Project supported by the National Key Research and Development Program of China (Grant No. 2017YFB0701502).

†Corresponding author. E-mail: cywang@mail.tsinghua.edu.cn



Ru a weak Al-site preference, which are consistent with reported results.<sup>[11–13]</sup>

**Table 1.** Normalized substitute formation energies of the main alloying elements in Ni<sub>3</sub>Al.

Element	Co	Cr	Mo	Re	Ru	Ta	W
$\bar{E}_{Al \rightarrow Ni}^X$	0.302	1.579	2.069	1.857	0.854	2.406	2.282

### 3.2. Stacking fault energy

Based on the site preference results in Subsection 3.1, five models include 14 layers or 16 layers of ideal packed were used in the calculation of SFEs, as shown in Fig. 1. The SFE is given by

$$\gamma_{SF} = \frac{E_{SF} - E_{ideal}}{A}, \quad (6)$$

where  $E_{SF}$  is the total energy of the stacking fault model,  $E_{ideal}$  is the total energy of the model with an ideal stacking sequence, and  $A$  refers to the cross-sectional area, perpendicular to the close-packed direction. In the calculation of SISF energies, the energies of the models with 14 layers ideal stacking sequence (Ideal 14) are calculated. In the calculation of SESF and SISF2 energies, the energies of the models with 16 layers ideal stacking sequence (Ideal 16) are calculated. The SISF and SESF energies of Ni<sub>3</sub>Al are 44.65 mJ/m<sup>2</sup> and 184.27 mJ/m<sup>2</sup>, respectively, which agrees with published data.<sup>[4]</sup> It should be pointed out that the type and concentration of the elements have an effective effect on the elastic properties of the systems. Furthermore, the calculation and experiment methods may also affect the results. So, some of our calculation results may have a little difference with the early reported experiment and calculation results.

Firstly, the alloying elements are located on the fault planes in Ideal 14, SISF, Ideal 16, SESF, and SISF2 models (*i.e.*, on layers 3, 3, 5, 5, and 5 in Fig. 1, respectively). The results of Fig. 2 show that Co and Ru with Ni-site occupation could decrease the SFEs, while the main refractory elements with Al-site occupation could increase the SFEs, except for Ru with Al-site occupation with an SESF of 110.39 mJ/m<sup>2</sup>. From Fig. 2, the SISF2 energies exceed the SISF energies, which means that a wide stacking fault corresponds to a high SFE. Compared with pure Ni<sub>3</sub>Al, Ru occupied the Al-site on the stacking fault plane leading to SESF decreasing to 73.88 mJ/m<sup>2</sup>, SISF increasing to 15.99 mJ/m<sup>2</sup>, and SISF2 increasing to 22.07 mJ/m<sup>2</sup>.

Furthermore, the segregation of elements was also considered, including Re, and Co–Ni, occupy layers 0 to 9. In Fig. 3, omitting sites near the vacuum layers, the relationship between alloying elements and the layer numbers of Re is symmetric, and SFEs increases near the SF while decrease apart from the SF. This shows that the SFEs are closely related to the specific location of the alloying, such as Re, W, Cr, and Ta. Co could decrease the SFEs on all calculated locations, and SISF energies are between 13 mJ/m<sup>2</sup> and 19 mJ/m<sup>2</sup>,

SESF energies are between 135 mJ/m<sup>2</sup> and 156 mJ/m<sup>2</sup>, and the fluctuation of the SFEs with changing location of Co is negligible.

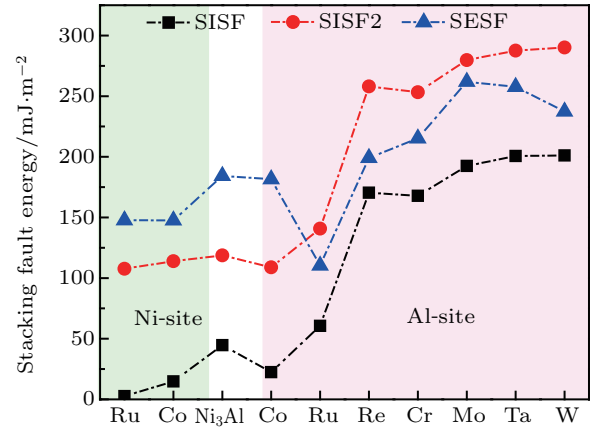


**Fig. 2.** Alloying effect on the energies of SISF, SISF2, and SESF. The green zone represents the energy results when elements occupy an Ni-site on the stacking fault plane, while the pink zone represents occupation of an Al-site on the stacking fault plane.

The energies of SISF2-types are higher than the SISF-types planar faults in Fig. 2, which suggests that a planar fault with a double AB repeat unit is harder to form than a simple AB planar fault defect. Compared with the SESF, the energies of SISF2 are lower than SESF in pure Ni<sub>3</sub>Al, but the energies of SISF2 are higher than SESF when alloying elements are located at an Al-site, except Co. In other words, with added alloying elements, the formation trend of the SISF2 and SESF changed. An SESF is easier than double-packed SISF with main alloying elements located near the planar fault.

**Table 2.** Alloying effect on the SISF ( $\gamma_{SISF}$ , in unit mJ/m<sup>2</sup>), SESF ( $\gamma_{SESF}$ , in unit mJ/m<sup>2</sup>), and SISF2 ( $\gamma_{SISF2}$ , in unit mJ/m<sup>2</sup>) energies of Ni<sub>3</sub>Al.  $X(Ni)$  represents element X occupying Ni site in the Ni<sub>3</sub>Al models, and  $X(Al)$  represents element X occupying Al site in the Ni<sub>3</sub>Al models.

	SISF	SESF	SISF2
Ni <sub>3</sub> Al	44.65	184.27	118.77
	68 <sup>a</sup> , 62 <sup>b</sup> , 37 <sup>c</sup>	89 <sup>a</sup> , 74 <sup>b</sup> , 152 <sup>c</sup>	
Co(Ni)	22.42	181.53	108.93
	64 <sup>a</sup> , 35.8 <sup>c</sup>	63 <sup>a</sup> , 148.8 <sup>c</sup>	
Co(Al)	26.16	94.48	111.66
	80 <sup>a</sup>	71 <sup>a</sup>	
Ru(Ni)	33.12	185.11	103.93
Ru(Al)	60.64	110.39	140.84
Ta(Al)	200.66	257.72	287.59
	118.6 <sup>c</sup>	191.6 <sup>c</sup>	
Cr(Al)	167.83	215.19	253.23
	107.7 <sup>c</sup>	171.7 <sup>c</sup>	
Re(Al)	170.36	258.08	199.11
	128 <sup>a</sup>	108 <sup>a</sup>	
Mo(Al)	192.51	279.73	261.90
	141 <sup>a</sup>	106 <sup>a</sup>	

<sup>a</sup>Ref. [14], calculation results by using supercells without vacuum, with alloying concentration 1.6 at.%; <sup>b</sup>Ref. [15], calculation results by slip model with a vacuum region; <sup>c</sup>Ref. [4].

The energies of double-packed SISF are higher than those of normal SISF and SESF with a third element located at an

Al-site near the stacking fault (except Co), although the energies of the double-packed SISF are lower than those of the SESF energies in pure  $\text{Ni}_3\text{Al}$ , but are lower than SESF with added alloying elements.

The above calculations of the doping effects on the stacking fault energies are concentrated on the different alloying types and the elements which are mainly aligned on the stacking fault planes. A further calculation evinces the relationship between alloying element location and the SFs, which can

be used in the analysis of the effect of Suzuki<sup>[16]</sup> in the  $\gamma'$  phase of Ni-based superalloys. From Fig. 3, the SFEs show a quasi-symmetrical distribution with the distance between the alloying elements and the SF layers. Re, Ta, and W decrease SISF2 and SESF energies when sat apart from the stacking fault layer, although they increase SFEs when located on the stacking fault planes. Moreover, Co occupation of an Ni-site decreases SFEs on the layers considered in these models.

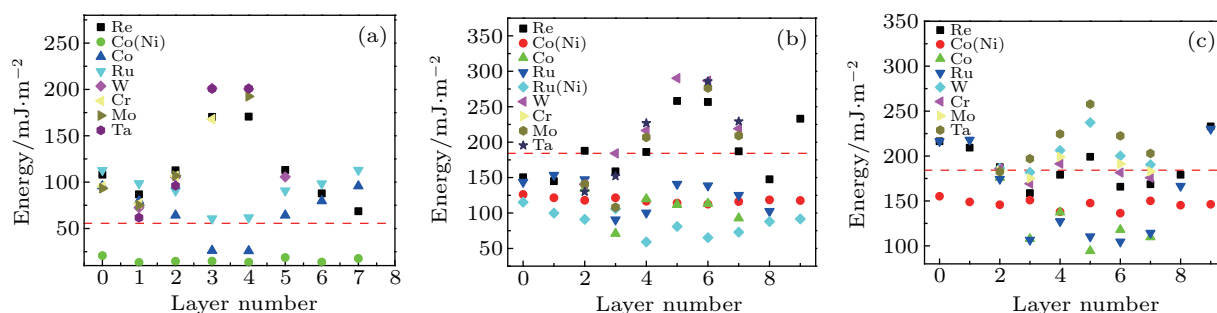


Fig. 3. Relationships between the alloying sites (layer number) and the SFEs. (a) SISF, (b) SISF2, and (c) SESF. The number of layers is consistent with that of the models illustrated in Fig. 1.

### 3.3. Electronic structural analysis

The doping effects on the SFEs are closely related to the interactions among near atoms and even near layers. The charge distributions and bonding characteristics of the models warrant more detailed analysis; the recent development of NiCo-based superalloys confirms the effect of Co elements on the alloy,<sup>[17]</sup> as being concentrated at high concentrations,<sup>[18]</sup> and the Co concentration in a real superalloy is higher than that used in this model. Here, the origin of the Ru effect was analyzed as it is the key element in the development of Ni-based superalloys.<sup>[1]</sup>

$\text{Ni}_3\text{Al}$  is an ideal  $L1_2$  crystal structure, and the charge accumulation tends to be located at the octahedral interstices, not at tetrahedral interstices, as shown in Fig. 4(a), which is consistent with charge accumulation of the pure fcc crys-

talline Al.<sup>[19]</sup> When an SISF effect is induced, the layer packed sequence changes, and then the charge tends to be located parallel along the close-packed [111] direction, as shown in Fig. 4(b) where layers 3 and 4 contain the faults. When a doubled-packed SISF is induced concurrently, the charge accumulation around the four defective layers (layers 4, 5, 6, and 7), tends to be parallel to the close-packed [111] direction, as shown in Fig. 4(c). In the SESF, the inserted layer (layer 5) has a different packed layer nearby with an environment like that of the same  $L1_2$  structure. Figure 4 also shows that the charge accumulation is closely correlated with its environment, and the nearest layer packing sequence makes the main contribution thereto. In other word, the SF changes the layer sequence, which causes the changes in the surrounding atomic environment and charge distribution.

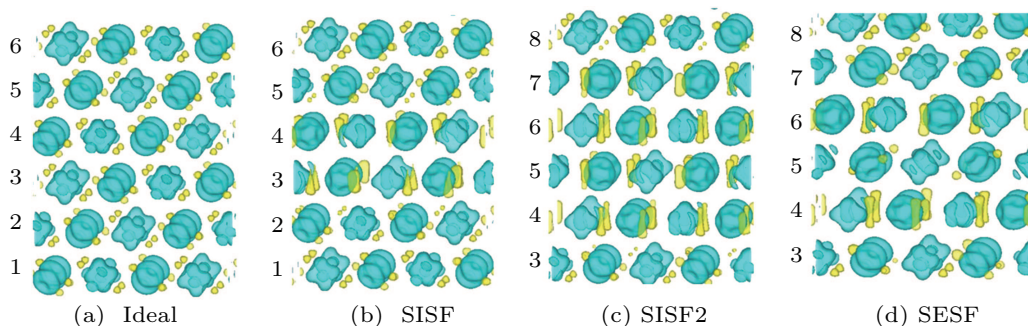


Fig. 4. Charge difference of  $\text{Ni}_3\text{Al}$  with (a) Ideal 16 layers, (b) SISF, (c) SISF2, and (d) SESF. The iso-surface is  $0.0075 \text{ eV}/\text{\AA}$ . The atoms in blue planes have different charge accumulations. Numbers 1 to 8 represent layer number in the models shown in Fig. 1.

After knowing the SFEs in  $\text{Ni}_3\text{Al}$ , a detailed analysis of the main element Ru addition in different SFs (Fig. 5) is presented. The addition of Ru, with strong charge accumulation around it, corresponds to strong bonding. In the anal-

ysis of pure  $\text{Ni}_3\text{Al}$ , the neighboring environment among the layers potentially corresponds to different charge distributions (hence atomic configurations). In Ideal 14 and layer 5 of SESF, the atoms have an identical neighboring environment, and the

charge distribution near the Ru displays a cubic-like distribution. The microscale charge distribution is consistent with its macroscale symmetry. The cubic structure has three 3-fold rotational symmetric axes, and the corresponding charge accumulation around Ru also shows the same rotational symmetry (Figs. 5(a) and 5(d)). This has been used in the calculation of the elastic properties when staining acts on the system.<sup>[20]</sup> In the SISF and SISF2 models, the environment around the Ru is identical to that in an hcp crystal, with ABAB as its repeat unit. As is known, the hcp structure has only one 3-fold rotational symmetry. The charge accumulation near Ru in SISF and SISF2 also shows only one 3-fold rotational symmetry (Figs. 5(b) and 5(d)), and the three accumulated parts display a 3-fold rotational symmetry along the [111] direction; *i.e.*, the [111] direction is a 3-fold axis of symmetry.

While the charge difference iso-surface allows visualization of the charge accumulation and the interaction among atoms, local density of state (LDOS) shows the bonding character in the energy space. Figure 5 also shows the detailed LDOS of Ru and its nearest neighbor Ni atoms. The LDOS shows a close correlation between Ru and its neighboring Ni atoms. The correlation could be divided into two parts, shown in grey and purple: the grey zone in Fig. 5 shows that the LDOSs have hybrid peaks due to hybridization between the two atoms. The hybrid characteristics corresponds to a covalent-like bonding, as discussed elsewhere. The purple zone in Fig. 5 shows that the LDOSs have complementary

characteristics, which means that, when Ru LDOS reaches a peak, the corresponding Ni LDOS reaches its valley, or *vice versa*. The characteristics evinces a polar bond (or ionic-like bond). The purple zone shows charge depletion and accumulation on specified atoms, in other words, an ionic-like bond, or polar bond. Ideal 16 and SESF have identical charge accumulation corresponding to the wide ionic-like bonding characteristics (the purple zone in Fig. 5): SISF and SESF have a narrow ionic-like bonding characteristics.

We now provide quantitative analyses, including the effects of charge transfer and structural energy. As the charge transfer is correlated with orbital interaction among atoms,<sup>[21]</sup> we integrate the DOS of lattice site<sup>[21,22]</sup>

$$N_l = \int_{-\infty}^{E_f} \sum_{\alpha} n_{\alpha l}(E) dE, \quad (7)$$

where  $n_{\alpha l}(E)$  represents the density of state at energy  $E$ ,  $\alpha$  are the sum of all the orbitals.

Then, the valence–electron occupancy at site  $l$  is

$$Q_l = 2N_l. \quad (8)$$

The charge transfer at lattice site  $l$  is

$$\Delta N_l = N_l^V - N_l. \quad (9)$$

The charge transfer is closely related to the orbital interaction among atoms.

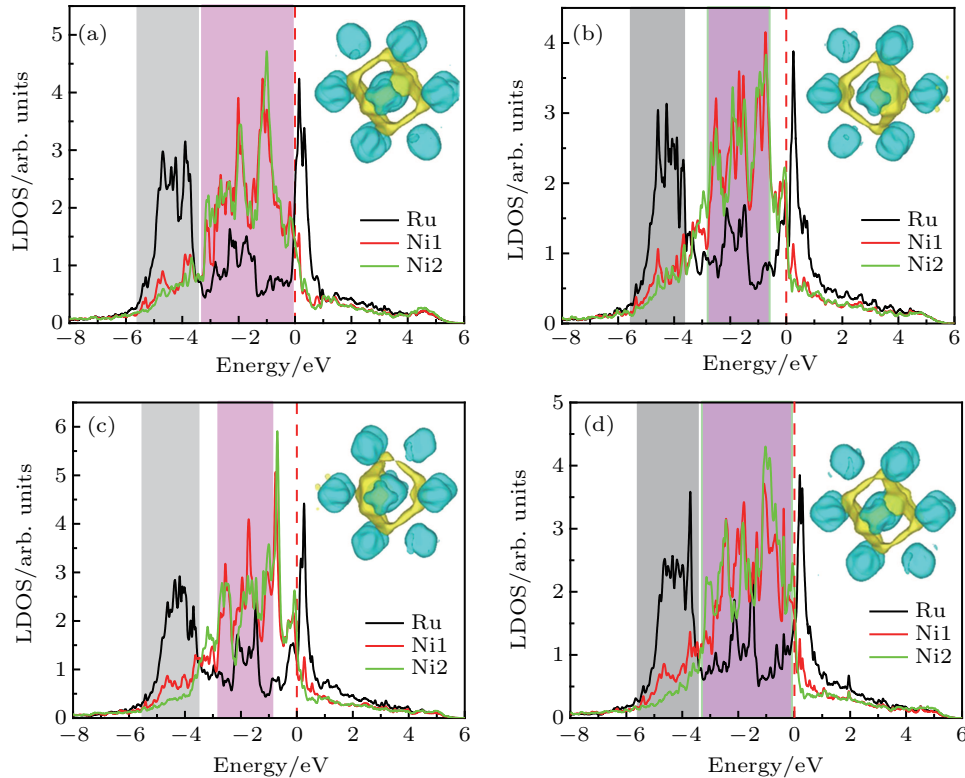


**Fig. 5.** Local density of state and charge difference of Ru in (a) Ideal 16, (b) SISF, (c) SISF2, and (d) SESF models, respectively. The local density hybridization of Ru occurs in SESF structures with its neighboring Ni. Charge accumulation of Ru with its 12 nearest neighbor atoms is illustrated. The iso-surface is 0.008 eV/Å. Ni1 and Ni2 are the nearest neighbor Ni atoms of Ru.

From Table 3, for Al elements with three electrons outside, the depletion of charge is more than 2, showing a totally metallic cohesive character between it and Ni. The charge depletion in an ideal structure is higher than that in SF, and that in SESF is the lowest. The total charge transfer of elements occupying Ni-site is mostly positive, except Ru. The total charge transfer of Ru occupying Ni-site is negative, because it has fewer electrons than those in Ni atom. The interaction between Ru and Al is weak.

**Table 3.** Total charge transfer at site l of elements in different models. Al and Ru represent that at the Al-site in Ni<sub>3</sub>Al, Ru(Ni) represent, Ru at the Ni-site in Ni<sub>3</sub>Al.

Element	Ideal 14	SISF	Ideal 16	SESF	SISF2
Al	2.1286	2.1251	2.1302	2.1174	2.1268
Ru	0.0050	0.0306	0.0174	0.0143	-0.0183
Ru (Ni)	-0.3204	-0.3465	-0.3096	-0.4453	-0.3340

The alloying effect on SFE can be correlated with structural energy. The structural energy  $E_1$  at site l<sup>[21]</sup> is

$$E_1 = \int_{-\infty}^{E_F} E \sum_{\alpha} n_{\alpha l}(E) dE, \quad (10)$$

where  $E_F$  is the Fermi energy, and  $n_{\alpha l}(E)$  is the local density of state at site l of the  $\alpha$  orbital. Here, all of the Fermi energy has shifted to zero. The structural energy can be considered in an analysis of why the charge accumulation of Ru in the SESF layer changes so little but does so with high SFEs. The structural energy difference between SF and the ideal model of Ru at the Al-site is lower than the energy difference of Al in pure Ni<sub>3</sub>Al (Table 4). In SESFs, the charge distribution changes little as the nearest neighbor conforms to an L1<sub>2</sub> structure, but the other near-neighbor layer can affect the structural energies and change the SFEs.

**Table 4.** The structural energy (in unit eV) of Ru in different models and sites. Al and Ru represent doping at the Al-site in Ni<sub>3</sub>Al, Ru(Ni) represents Ru at the Ni-site in Ni<sub>3</sub>Al.

Element	Ideal 14	SISF	Ideal 16	SESF	SISF2
Al	-1.379	-1.386	-1.380	-1.387	-1.397
Ru	-1.477	-1.418	-1.465	-1.423	-1.434
Ru(Ni)	-1.407	-1.433	-1.406	-1.454	-1.430

The electronic structural analysis shows that the SFEs are closely related to the neighboring layer environment which affects the charge distribution and charge transfer. In structural energy terms, the changes in the relative position of the layer result in the SISF, SISF2, and SESF having symmetry reduction of their charge accumulations, from three 3-fold rotational symmetries to one 3-fold rotation symmetry, about 2, 4, and 2 layers, respectively. From the perspective of bonding, this evinces the reduction of ionic-like bonding characteristics, but covalent-like bonding characteristics change little. The specific bonding charge is the sum of the calculated charge trans-

fers. The SESF energies and the corresponding structural energies illustrated that the SFEs are not only a nearest neighbor layer interaction, but also a holistic interaction.

## 4. Conclusion

The alloying effects on the SFEs in Ni<sub>3</sub>Al were calculated with the first principles study from both an energetic and electronic structural analysis perspective. The conclusions are as follows:

(i) From the sight of formation energy, the main elements prefer to occupy the Al-site in Ni<sub>3</sub>Al to strengthen that phase of the Ni-based superalloys, but Co and Ru show weak site preferences.

(ii) Both element type and location can affect the SFEs. Co and Ru can decrease the SFEs while other main elements increase the SFEs.

(iii) The energies of SISF2 are lower than those of SESF with the main alloying elements (except Co addition) located at the Al site on the stacking fault planes, though SESF is lower than that of SISF2 in a pure Ni<sub>3</sub>Al model.

(iv) The electronic structure analysis of Ru addition shows that both reductions of the symmetry of charge redistribution and the changes of structural energies will affect the SFEs.

## References

- [1] Reed R C 2008 *The superalloys: fundamentals and applications* (Cambridge: Cambridge University Press)
- [2] Yokokawa T, Harada H, Mori Y, Kawagishi K, Koizumi Y, Kobayashi T, Yuyama M and Suzuki S 2016 *Proceedings of the 13th International Symposium of Superalloys*, pp. 123-130
- [3] Yu X X and Wang C Y 2012 *Mater. Sci. Eng. A* **539** 38
- [4] Rao Y, Smith T M, Mills M J and Ghazisaeidi M 2018 *Acta Mater.* **148** 173
- [5] Kresse G and Hafner J 1994 *J. Phys.: Condens. Matter* **6** 8245
- [6] Zhang W, Lin J, Xu W, Fu H and Yang G 2017 *Tsinghua Sci. Technol.* **22** 675
- [7] Blöchl P E 1994 *Phys. Rev. B* **50** 17953
- [8] Perdew J P, Burke K and Ernzerhof M 1996 *Phys. Rev. Lett.* **77** 3865
- [9] Wagner C and Schottky W J Z 1930 *Phys. Chem. B* **11** 171
- [10] Ruban A V and Skriver H L 1997 *Phys. Rev. B* **55** 856
- [11] Jiang C and Gleeson B 2006 *Scr. Mater.* **55** 433
- [12] Liu S H, Wen M R, Li Z, Liu W Q, Yan P and Wang C Y 2017 *Mater. & Des.* **130** 157
- [13] Wen M and Wang C 2018 *Phys. Rev. B* **97** 024101
- [14] Eurich N and Bristowe P 2015 *Scr. Mater.* **102** 87
- [15] Voskoboinikov R 2013 *Phys. Met. Metallogr.* **114** 545
- [16] Suzuki H 1962 *J. Phys. Soc. Jpn.* **17** 322
- [17] Suzuki A, Inui H and Pollock T M 2015 *Ann. Rev. Mater. Res.* **45** 345
- [18] Titus M S, Eggeler Y M, Suzuki A and Pollock T M 2015 *Acta Mater.* **82** 530
- [19] Nakashima P N H, Smith A E, Etheridge J and Muddle B C 2011 *Science* **331** 1583
- [20] Kioussis N, Herbranson M, Collins E and Eberhart M E 2002 *Phys. Rev. Lett.* **88** 125501
- [21] Wang C Y, Liu S Y and Han L G 1990 *Phys. Rev. B* **41** 1359
- [22] Wang C, Yue Y and Liu S 1990 *Phys. Rev. B* **41** 6591